MATHEMATICS

The Euler spiral of rat whiskers

Eugene L. Starostin[1,2], Robyn A. Grant[3], Gary Dougill[3],
Gert H. M. van der Heijden[2], Victor G. A. Goss[1]*

This paper reports on an analytical study of the intrinsic shapes of 523 whiskers from 15 rats. We show that the variety of whiskers on a rat's cheek, each of which has different lengths and shapes, can be described by a simple mathematical equation such that each whisker is represented as an interval on the Euler spiral. When all the representative curves of mystacial vibrissae for a single rat are assembled together, they span an interval extending from one coiled domain of the Euler spiral to the other. We additionally find that each whisker makes nearly the same angle of 47° with the normal to the spherical virtual surface formed by the tips of whiskers, which constitutes the rat's tactile sensory shroud or "search space." The implications of the linear curvature model for gaining insight into relationships between growth, form, and function are discussed.

INTRODUCTION

Over the past few decades, the rat's set of mystacial vibrissae (whiskers) has become prototypic for exploring links between synaptic circuits and behavior (Fig. 1, A and B) (1). This interest emerged when Woolsey and van der Loos (2) described, in 1970, the curious and remarkable one-to-one somatotopic mapping between the linearly arranged whiskers on a mouse's cheek and the primary somatosensory "barrel cortex," i.e., each whisker is represented by a discrete and well-defined structure in a section of the animal's brain. That arrangement was later found to exist in the rat and many other rodents (1). Evidently, vibrissae have evolved into long slender flexible structures well adapted to operate as tactile sensors (Fig. 1C).

That form-to-function relation must be the key to our understanding of the rat's tactile processing system. As Thompson (3) emphasized, mathematical analysis of form plays an important role in providing information about biological function. In the case of whisker sensory systems, the extent to which a geometric description helps us depends on its ability to capture the inherent morphological properties of each whisker.

During their functioning, whiskers change shape by bending, i.e., by varying their curvature. Therefore, the geometric description should primarily account for how they are curved. We show that whisker centerlines are well approximated by a curve with linear curvature corresponding to an interval of a universal Euler spiral, a mathematical curve first defined by Euler in 1744 (Fig. 2) (4).

Rats are highly dependent on their whisker touch system when exploring their surroundings. By dabbing and stroking their whiskers over a surface, a rat can determine an object's shape, size, orientation, and texture, much like how humans use their fingertips (5). Specifically, reaction forces and moments at the base of the whisker are processed by sensory areas in the rat brain (6, 7). On each of the rat's mystacial pads, the 30 most prominent whiskers are arranged in ordered five rows and seven columns. That grid-like layout of the pad is mirrored in physical structures in the somatosensory cortex, termed "barrels" (2), as well as in the brainstem and thalamus (1).

The brain is thought to encode tactile signals arising from forces and moments within the whisker follicles (8, 9). Before attempting to interpret the neuronal signals themselves, it is imperative to have knowledge of those forces and moments when the whisker shaft is deflected and bent upon contact with an object. The size and natural shape of each whisker, including its taper and intrinsic curvature, strongly influence the manner in which it deforms, and therefore, the tactile signals in the follicle. It is known that rats exploit intrinsic curvature to their advantage (10, 11).

One line of current research focuses on formulating predictive models of the mechanics of whiskers, i.e., deflections of the shaft and the corresponding reaction forces and moments at the base (11–18). In developing these models, we are mindful that their appropriateness to neuroscience, robotics, and other applications will depend on how well they account for the material and geometrical properties of the whisker shaft.

Many mechanics studies have proceeded on the basis of two assumptions. First, as whiskers are long slender structures, with one dimension (length) considerably larger than the other two, the form of a rat vibrissa can be approximated by its centerline (Fig. 1C) (19, 20). Second, the intrinsic form of the centerline is essentially planar; inspection of data obtained from measurements of rat vibrissae indicates that torsion, which quantifies the departure of the centerline curve from a
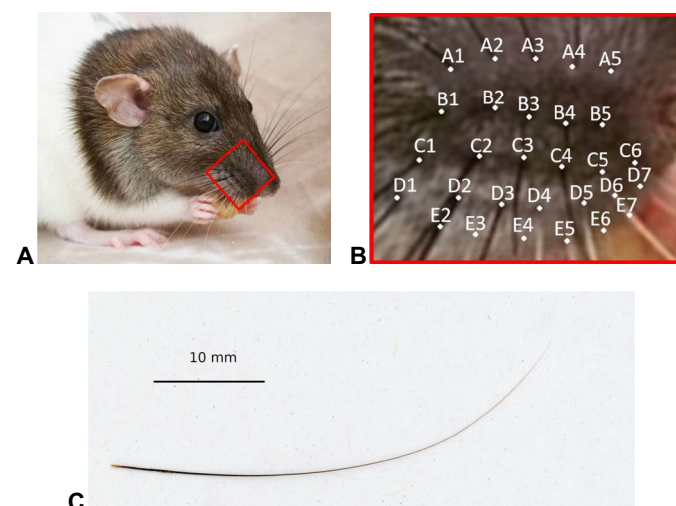
Fig. 1. A rat and its whiskers. (**A**) A photograph of a rat (photo credit: Maria Panagiotidi, University of Salford). (**B**) The mystacial pad with labeled locations of the base points of 30 whiskers at the right side of a rat. The mystacial pad matrix has five rows (A to E) and seven columns (1 to 7); for five entries, the whiskers are absent. (**C**) A two-dimensional scan of a whisker.

[1]School of Engineering, London South Bank University, 103 Borough Rd., London SE1 0AA, UK. [2]Department of Civil, Environmental and Geomatic Engineering, University College London, Gower St., London WC1E 6BT, UK. [3]Division of Biology and Conservation Ecology, Manchester Metropolitan University, Chester St., Manchester M1 5GD, UK.
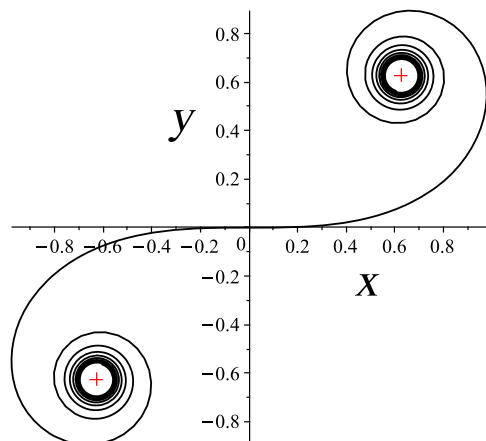*Corresponding author. Email: gossga@lsbu.ac.uk

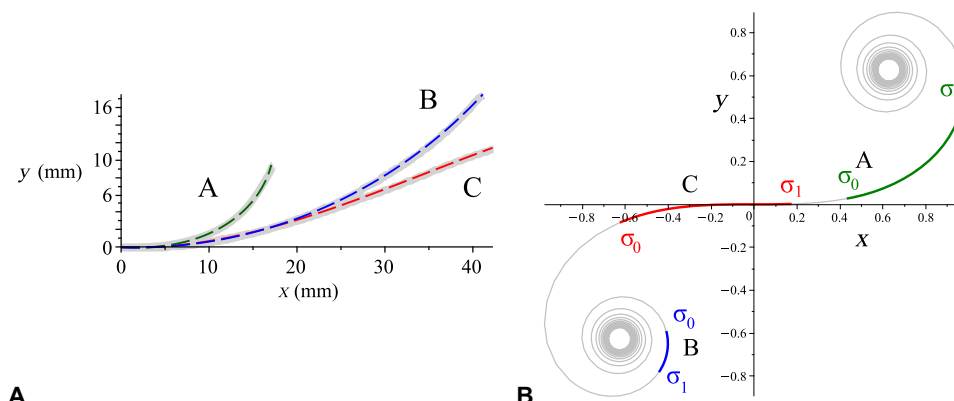plane, is small and the median of this departure is 0.1% of whisker length (13, 15).

RESULTS
Fitting the data
We examine the curvature of the centerlines of two independent datasets of experimentally measured vibrissae belonging to 15 brown rats *Rattus norvegicus*: (i) dataset I obtained by the authors (167 whiskers of eight rats) and (ii) dataset II by courtesy of Hartmann and colleagues (21) (356 whiskers of seven rats). Each rat is identified with a number: 1,4-10 (dataset I) and 11-13,16-19 (dataset II). There are some pertinent qualitative points to emphasize that give support to the Euler spiral model. These stem from a visual inspection of the scanned rat vibrissae:

1) Many vibrissae tend to have either noticeably (to the human eye) increasing or decreasing curvature—they either straighten out or start to curl up;

2) Most vibrissae have curvature of the same sign, however, a notable proportion curve one way and then the other way, i.e., they contain an inflection point;

3) We do not observe any rat vibrissa with more than one significant interior inflection point, i.e., we do not find whiskers that undulate (such as a sine wave).

It follows that a constant curvature (circular) approximation is too crude to depict the variety of forms of vibrissae, while a high degree polynomial curvature function is unnecessarily complicated. Rather, a two-parameter linear curvature function encompasses the diversity of vibrissae morphologies that we observe. Consequently, we fit the data to Euler spirals, given by the Cesàro equation $\kappa(\hat{s}) = A\hat{s} + B$, where $\hat{s} \in [0, 1]$ is the scaled arc length, κ is the curvature, and A and B are constants, called the Cesàro coefficients [see the supplementary materials in (13) and Materials and Methods]. The dataset initially contained $167 + 356 = 523$ whiskers, 7 of which (2 and 5, respectively) were discarded as having residual standard deviation (RSD), normalized by length, larger than 0.8% (see "Details of Results" section in the Supplementary Materials and fig. S1).

Conformal mapping of the whiskers onto the universal Euler spiral
Three exemplar whiskers A, B, and C are shown in Fig. 3A, where the Euler spiral approximations are superimposed onto the experimentally measured curves. These three Euler spiral intervals were rescaled and placed on their corresponding intervals of the universal Euler spiral (Fig. 3B). Each is characterized by a pair of shape parameters σ_0 and σ_1 specifying the arc length coordinates of the end points of the intervals on the universal spiral. We calculate σ_0 and σ_1 for all whiskers, and we draw all the representing intervals of the spiral, $[\sigma_0, \sigma_1]$, each shifted in the vertical direction according to its whisker index, above the universal spiral (Fig. 4A). In addition, the distribution of the shape parameters σ_0 and σ_1 is presented in the parametric plane in Fig. 4B. We can see that the set of whiskers of a given individual animal, when taken together, tends to occupy an interval of the universal Euler spiral extending from one coiled domain to the other (this is more apparent for individuals that are represented by larger numbers of whiskers in our datasets) (Fig. 4A). Speaking metaphorically, the whiskers on a rat's cheek together compose the Euler spiral.

The dimensional Euler spiral approximations for all whiskers, as well as the mean shapes (represented as Euler spirals having the mean

Fig. 2. The normalized Euler spiral. The crosses mark the limit points $x = y = \pm\sqrt{2\pi}/4$.

A

B

Fig. 3. Mapping whiskers onto the Euler spiral. (**A**) Three exemplar whiskers approximated by Euler spirals (in millimeters) are shown in dashed color over the original data (thick gray). (**B**) The same three whiskers conformally mapped onto the universal Euler spiral (the base ends are marked with σ_0 and the tips with σ_1). The green whisker (A) has a noticeably increasing curvature and is mapped onto the right. The blue whisker (B) has the most uniform (but slightly decreasing) curvature, and it appears on the left part of the spiral. The red whisker (C) has an inflection close to its tip and hence passes through the origin. In placing them on the Euler spiral, the three whiskers are individually scaled.

values of the Cesàro coefficients) for each position at the mystacial pad, are shown in Fig. 5 (see also fig. S6).

We see that, for two-thirds of the occupied positions on the mystacial pad, the mean curve has curvature that decreases from base to tip.

The shroud: Arrangement of the whiskers in three-dimensional space

The virtual surface formed by the tips of a rat's mystacial vibrissae constitutes a tactile sensory shroud (hereafter "shroud"). To model it, we
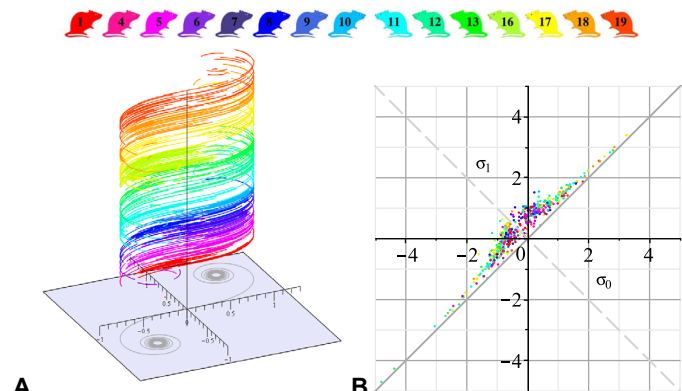

Fig. 4. Whisker shapes and shape parameters, 516 whiskers for 15 rats, each animal painted in its reference color. (**A**) Individually layered 516 whisker shapes mapped onto intervals of the universal Euler spiral shown in gray underneath. See fig. S7 for the whisker density map. (**B**) The parametric plane (σ_0, σ_1). All points lie above the diagonal $\sigma_1 = \sigma_0$. Shapes with $\sigma_0 < \sigma_1 < 0$ ($0 < \sigma_0 < \sigma_1$) have decreasing (increasing) curvature and have no inflections. Shapes with $\sigma_0 \leq 0 \leq \sigma_1$ are inflectional; among them, there are more with $\sigma_1 < -\sigma_0$ (below the dashed diagonal), i.e., with the inflection point closer to the tip than to the base.

follow the procedure proposed in (13) and use the coordinates of the whisker base points and the corresponding angles of emergence from (22) (Fig. 6A). The shape of each of 30 whiskers is now represented as a Euler spiral having the mean values of the Cesàro coefficients for given position at the mystacial pad (see fig. S6). The shroud is well approximated by an ellipsoid centered in the animal's symmetry plane. This ellipsoid is close to a sphere, and it is known that its center lies in the middle of a chord connecting the animal's eyes (23). Table 1 presents the mean angles (in degrees) for 15 rats, between the whisker tip tangent vectors and the normals to the ellipsoidal surface at the points closest to the tips (see Fig. 6B).

The average value is equal to 47° for the entire set and 48° for the interior submatrix (boldfaced values in Table 1, obtained by removing rows 1 and 5 and columns 1 and 7). We note that the average angle between tangents to the whiskers at their bases and normals to the surface of the mystacial pad is smaller, 33°. The SD is 5. 2° (2. 5° for the interior submatrix), which is relatively small, so the angle is practically constant. Because of the near sphericity of the shroud, the whisker tip tangents make nearly the same aforementioned angle with vectors originating at the sphere's center (located midway between the eyes) and directing to the whisker tips.

DISCUSSION
In showing that the generic shapes of rat whiskers are well approximated by the Euler spiral, we conjecture that this is a manifestation of linear laws underpinning rat vibrissae growth [akin to the logarithmic spirals of sea shells that can be explained by a simple growth rule (3); note that for the logarithmic spiral, it is the radius of curvature that is a linear function of arc length, whereas the Euler spiral is a curve with linear curvature].
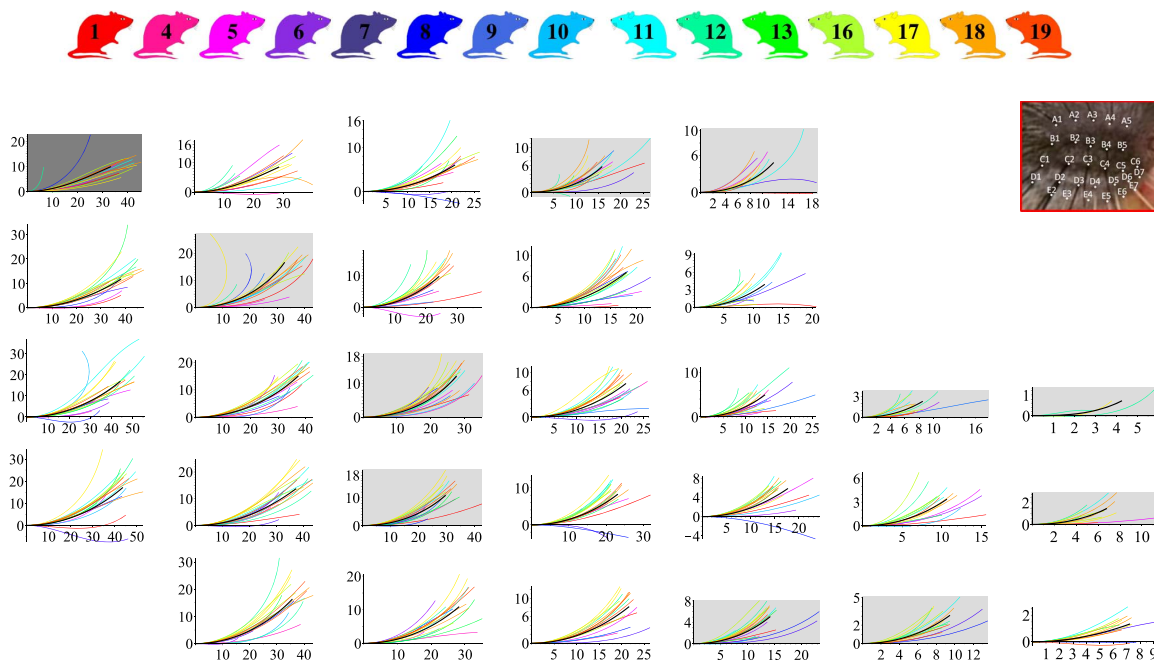
Fig. 5. Euler spiral approximations of whisker planar shapes presented in the form of the mystacial pad matrix (30 entries, 5 rows, and 7 columns) (see Fig. 1B, repeated in the upper right corner). Colors mark 15 different animals (same as in Fig. 4). Black curves show mean Euler spiral approximations. The coordinate axes are marked in millimeters. The dark and light gray backgrounds correspond to the matrix entries where the mean Euler spirals have an inflection point (dark) and where their curvature increases from base to tip (light).
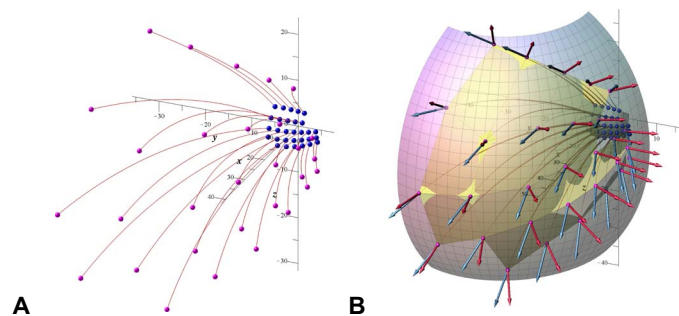
Fig. 6. Configuration of the right side of the whisker sensory shroud. The origin 0,0,0 is placed at the mean position of all whisker basepoint locations (for both mystacial pad vibrissae), the y axis points rostrally, and the negative y axis points caudally, the xy plane is the average whiskerrow plane, and the yz plane is the sagittal plane. (**A**) Each of the 30 whiskers is represented by a Euler spiral; the blue balls mark the base points at the rat's mystacial pad, and the pink balls show the tips. (**B**) The surface spanned by the whisker tips (yellow) is approximated by an ellipsoid (transparent). Arrows show tangent vectors (light blue) at the tips and normals (red) to the ellipsoidal surface at points closest to the tips; the normals are shifted to the corresponding tips. See three-dimensional interactive in figs. S8 and S9.

Table 1. The angles (in degrees) between the whisker tip tangents and the normals to the ellipsoidal approximation of the rat's sensory shroud (see Fig. 6B) for each position on the mystacial pad, averaged across the whole dataset.

	1	2	3	4	5	6	7
A	44	47	50	42	33		
B	42	**46**	**50**	**50**	49		
C	36	**42**	**48**	**50**	49	50	49
D	36	**43**	**49**	**50**	49	48	48
E		45	52	54	55	53	55

We assume that the shape, in particular, the intrinsic curvature of the centerline, of each portion of the whisker does not change after this portion leaves the follicle in the process of growth, i.e., vibrissal shafts are made of dead cells (24). It follows that segments of an individual vibrissa represent snap shots of different stages of its life cycle. It is known that both vibrissae length and width at the base grow linearly with time (for most of the growth phase) (25). That constant growth rate of whisker length infers a linear correspondence between centerline arc length and time (see fig. S10).

What makes vibrissae intrinsically curved is not known, but it is reasonable to think of a mechanism similar to that responsible for natural curling of hair. There exist two hypotheses for the origin of this curling (26). Both explain it by a geometric factor—newly born cells at one side of the whisker shaft take more volume than at the opposite side. Thus, an essential factor is a gradient of growth, i.e., of increase in volume occupied by cellular material, over the cross section of the hair or whisker at its base. Given linear correspondence between arc length and time, if the growth gradient were to be constant in time, then the vibrissa would curve at constant rate and its centerline would be a circular arc, whereas linear variation of the growth gradient in time produces a centerline with linear curvature. Furthermore, significant nonlinear variation of growth rates across the base would cause essential nonlinearities of the whisker curvature, which we have not observed.

Each whisker on the rat's mystacial pad can be viewed as a constitutive element of its tactile sensory system. The distribution of the whisker tips on the shroud surface is sufficiently dense such that any first whisker tip to come into contact with an external object will be at practically the same angle relative to the normal to the surface of that object (this may not be the case for the whiskers bordering the mystacial pad as they may approach the object sidewise; the latter may explain the smaller deviation from the mean angle for the whiskers forming the interior domain of the shroud) (see Table 1). The observed near constancy of that first contact point angle suggests that this is advantageous for the rat. As we see, that value turns out to be close to 45°, which lies midway between two extremes of orthogonal and tangential contact with the external surface (0° and 90°, respectively). While we observe the uniformity of this particular angle value, we cannot offer

an explanation, but we speculate that it relates to sensory function of vibrissae, i.e., it may be an evolutionary phenomenon. One can, nevertheless, assume that the positions of the whisker tips on the shroud together with their relative orientations are key factors in the functioning of the rat's vibrissal system. It follows that each whisker must have a shape that satisfies those tip conditions together with the conditions at its base (position on the mystacial pad and the angle of emergence). This problem is known as a two point G^1 Hermite interpolation. A shape with constant curvature will, in general, not achieve this, but linear variation of curvature appears to be sufficient (27). Note also that the Euler spiral serves as a minimizer of the L_2-norm of the variation of curvature (known as a minimum variation curve) $\int_0^L \left(\frac{d\kappa}{d\hat{s}}\right)^2 d\hat{s} \rightarrow \min$ (4).

It is clear that vibrissae forms can be accurately described in different coordinate systems (11, 13, 15). The benefit of referring directly to curvature as a function of arc length is that it provides a description independent of the position and orientation of the curve in the plane. The Euler spiral encompasses forms of vibrissae that have both increasing and decreasing curvatures along their lengths. It additionally embraces vibrissae that curve one way and then in the opposite direction, i.e., having an inflection point. All this suggests that the Euler spiral model captures essential features of whisker shapes, which is critical for understanding their function. Furthermore, we speculate that vibrissae of other mammals (in particular, terrestrial) follow similar rules and are also described by Euler spirals, which would be consistent with observations in (28). In that case, knowledge of distributions of the shape parameters σ_0 and σ_1 could be a useful tool to identify species.

MATERIALS AND METHODS
Data acquisition
All work in this study conformed to U.K. Home Office Regulations and was approved by local ethics committees at Manchester Metropolitan University. Two Long-Evans (animals 1 and 4) and six Sprague-Dawley rats (animals 5 to 10) were euthanized and frozen before this study. Rats were defrosted in 4% paraformaldehyde. Mystacial pads were dissected and soaked in 1% Lugol's iodine solution for 48 hours to ensure a consistent, high-contrast, dark whisker stain and enable whiskers to be imaged against a white background. Individual whiskers were identified and plucked from the pad. They were placed on the bed of an Epson V600 scanner (Epson, Tokyo) and scanned at 12,800 dots per inch for a pixel resolution of approximately 2 μm.

Mathematical modeling

In what follows, we give details of the mathematical procedure for fitting the Euler spiral to the experimental data for each whisker w ($w = 1, …, N = 523$). We start with an assumption that we have N_w data points $P_i = (X_i, Y_i)$, $i = 1, …, N_w$ (X, Y are Cartesian coordinates in the plane). We are searching for a universal description of the centerlines of vibrissae by approximating them by a plane model curve $C(\mathbf{p}) = \{\mathbf{r}(s) = (X(s), Y(s)), s \in \mathbb{R}^1; \mathbf{p}\}$. Here, s is the arc length along the centerline, and $\mathbf{p} \in \mathbb{R}^n$ is a vector of fitting parameters. The minimal distance from point P_i to the model curve is computed as $d_i := \min_{s_i \in \mathbb{R}} \sqrt{(X_i - X(s_i))^2 + (Y_i - Y(s_i))^2}$. For each whisker, we find the $\mathbf{p}$ that realizes $\min_{\mathbf{p}} \sum_{i=1}^{N_w} d_i^2$, thus $\mathbf{p}$ determines an estimate of the whisker's centerline. Let $s_0 := \min_{1 \le i \le N_w} (s_i)$; then, we define the length of the whisker by $L := \max_{1 \le i \le N_w} (s_i) - s_0$.

Following (13), we describe the signed curvature $\tilde{\kappa}(s)$ of the whisker's centerline as a linear function of arc length s such that the Cesàro equation is $\tilde{\kappa}(s) = \tilde{A}(s - s_0) + \tilde{B}$, $s \in [s_0, s_0 + L]$, and $\tilde{A} = \text{const}$, $\tilde{B} = \text{const}$. It is convenient to individually rescale all the centerlines (without affecting their shapes) by normalizing all lengths by L. Thus, we write $\kappa(\hat{s}) = A\hat{s} + B$, $\hat{s} := (s - s_0)/L$, $\kappa = \tilde{\kappa}L$, $A = \tilde{A}L^2$, $B = \tilde{B}L$, and $\hat{s} \in [0, 1]$. Without loss of generality, we assume $A \ge 0$ (if $A < 0$, then we simply change signs of both A and B, this being equivalent to switching to the mirror image of our curve or looking at a whisker from the other side of its plane). We first consider the case $A > 0$. The angle $\theta(\hat{s})$ between the x axis and the tangent to the centerline $\hat{\mathbf{r}}'(\hat{s}) = (\hat{x}'(\hat{s}), \hat{y}'(\hat{s})) = (\cos \theta(\hat{s}), \sin \theta(\hat{s}))$ (here and in the following, the prime denotes differentiation with respect to $\hat{s}$) is called the slope angle, and it satisfies $\theta'(\hat{s}) = \kappa(\hat{s})$. Integrating the latter, we immediately get $\theta(\hat{s}) = \frac{A}{2}\hat{s}^2 + B\hat{s} + \theta_0$. The coordinates are then expressed in terms of the Fresnel integrals $S(z) = \int_0^z \sin\left(\frac{\pi}{2}t^2\right)dt$ and $C(z) = \int_0^z \cos\left(\frac{\pi}{2}t^2\right)dt$ (29)

$$\hat{x}(\hat{s}) = \sqrt{\frac{\pi}{A}}(C(\zeta) \cos \alpha + S(\zeta) \sin \alpha)$$

$$\hat{y}(\hat{s}) = \sqrt{\frac{\pi}{A}}(S(\zeta) \cos \alpha - C(\zeta) \sin \alpha) \qquad (1)$$

where $\zeta := \frac{A\hat{s} + B}{\sqrt{\pi A}}$, $\alpha := \frac{B^2}{2A} - \theta_0$. Equation 1 describes a Euler spiral or clothoid (4).

We next show how one can give a universal form to the curve expressed by Eq. 1. We are free to direct our coordinate axes simply by choosing $\theta_0 = \frac{B^2}{2A}$ so that $\alpha = 0$. Next, we shift the origin of the arc length coordinate by introducing $\tilde{s} := \hat{s}_0 + \hat{s}$, $\hat{s}_0 = \frac{B}{A}$. Thus, $\tilde{s} \in \left[\frac{B}{A}, \frac{B}{A} + 1\right]$. Last, we rescale the curve by defining $\sigma := \sqrt{\frac{A}{2}}\tilde{s}$. The new arc length varies in the range $[\sigma_0, \sigma_1]$, $\sigma_0 = \frac{B}{\sqrt{2A}}$ and $\sigma_1 = \frac{B}{\sqrt{2A}} + \sqrt{\frac{A}{2}}$. The new coordinates are $x(\sigma) = \int_0^\sigma \cos(t^2)dt$ and $y(\sigma) = \int_0^\sigma \sin(t^2)dt$, which describe a universal Euler spiral (Fig. 2). We see that any original whisker centerline can be conformally mapped onto an interval lying on the universal Euler spiral with arc coordinates of the end points σ_0 and σ_1, which are simple functions of the coefficients A and B. Note that the shape of the centerline does not change except for homogeneous dilation (the scaling factor is $\sqrt{A/2}$). Consequently, curves with higher change of curvature (larger A) are represented by longer intervals on the Euler spiral.

When $A \to 0$, the curve approaches a circular arc for $B \ne 0$ or a straight line for $B = 0$. These two singular limits correspond to the points $(\text{sgn}(B)\sqrt{2\pi}/4, \text{sgn}(B)\sqrt{2\pi}/4)$ and $(0,0)$ (the only inflection point), respectively (Fig. 2). Approximation of an almost circular centerline pushes σ_0 and σ_1 to infinity and makes the normalized interval shorter. Straight centrelines ($A = B = 0$) are collapsed to the origin, near straight curves map to short intervals in its vicinity.

Data processing

Grayscale whisker images were thresholded to black and white, and the whisker outlines were determined using MATLAB's bwboundaries function. The Cartesian coordinates of the points at the boundaries constitute the dataset I. They were processed by the Maple 2017 Lowess (LOcally WEighted Scatterplot Smoothing) procedure and then resampled at a uniform grid of 100 abscissa points. The fragments of the whiskers corresponding to the follicles were cut off [≈7% of length (30)]. The same number ($N_w = 100$) of the Cartesian coordinates of the centerlines were processed for dataset II. Using the Maple 2017 NonlinearFit procedure, we fit the data to the dimensional Euler spiral as the model curve having three parameters $\mathbf{p} = (\tilde{A}, \tilde{B}, \theta_0)$. After that, the length L of each whisker was calculated (see figs. S3, A and B, and S4). The quality of the approximation was estimated by RSD. The union of datasets I and II initially contained $167 + 356 = 523$ whiskers, 7 of which (2 and 5, respectively) were discarded as having an RSD of $>0.008L$. We then computed the Cesàro coefficients A and B (see their distributions in figs. S3, C and D, S4, and S5) and the shape coefficients σ_0 and σ_1 (Fig. 4B). The mean values $<B>$ and $<A>$ (together with the mean lengths) were also found for each entry of the mystacial pad matrix (see fig. S6, A and B).

REFERENCES AND NOTES

1. K. Fox, T. Woolsey, *Barrel Cortex* (Cambridge Univ. Press, 2008).
2. T. A. Woolsey, H. van der Loos, The structural organization of layer IV in the somatosensory region (SI) of mouse cerebral cortex: The description of a cortical field composed of discrete cytoarchitectonic units. *Brain Res.* **17**, 205–242 (1970).
3. D. W. Thompson, *On Growth and Form* (Cambridge Univ. Press, ed. 2, 1942).
4. R. Levien, "The Euler spiral: A mathematical history" (Technical Report UCB/EECS-2008-111, Department of Electrical Engineering and Computer Sciences, University of California, Berkeley, 2008).
5. R. A. Grant, P. M. Itskov, R. B. Towal, T. J. Prescott, Active touch sensing: Finger tips, whiskers, and antennae. *Front. Behav. Neurosci.* **8**, 50 (2014).
6. S. J. Whiteley, P. M. Knutsen, D. W. Matthews, D. Kleinfeld, Deflection of a vibrissa leads to a gradient of strain across mechanoreceptors in a mystacial follicle. *J. Neurophysiol.* **114**, 138–145 (2015).

7. B. Mitchinson, K. N. Gurney, P. Redgrave, C. Melhuish, A. G. Pipe, M. Pearson, I. Gilhespy, T. J. Prescott, Empirically inspired simulated electro-mechanical model of the rat mystacial follicle-sinus complex. *Proc. Biol. Sci.* **271**, 2509–2516 (2004).

8. D. Campagner, M. H. Evans, M. R. Bale, A. Erskine, R. S. Petersen, Prediction of primary somatosensory neuron activity during active tactile exploration. *eLife* **5**, (2016).

9. D. Campagner, M. H. Evans, M. S. E. Loft, R. S. Petersen, What the whiskers tell the brain. *Neuroscience* **368**, 95–108 (2018).

10. A. E. Schultz, J. H. Solomon, M. A. Peshkin, M. J. Hartmann, in *Proceedings of the 2005 IEEE International Conference on Robotics and Automation* (IEEE, 2005), pp. 2588–2593.

11. B. W. Quist, M. J. Z. Hartmann, Mechanical signals at the base of a rat vibrissa: The effect of intrinsic vibrissa curvature and implications for tactile exploration. *J. Neurophysiol.* **107**, 2298–2312 (2012).

12. J. H. Solomon, M. J. Hartmann, Robotic whiskers used to sense features. *Nature* **443**, 525 (2006).

13. R. B. Towal, B. W. Quist, V. Gopal, J. H. Solomon, M. J. Z. Hartmann, The morphology of the rat vibrissal array: A model for quantifying spatiotemporal patterns of whisker-object contact. *PLOS Comput. Biol.* **7**, e1001120 (2011).

14. Y. S. W. Yu, M. M. Graff, M. J. Z. Hartmann, Mechanical responses of rat vibrissae to airflow. *J. Exp. Biol.* **219**, 937–948 (2016).

15. P. M. Knutsen, A. Biess, E. Ahissar, Vibrissal kinematics in 3D: Tight coupling of azimuth, elevation, and torsion across different whisking modes. *Neuron* **59**, 35–42 (2008).

16. J. H. Solomon, M. J. Z. Hartmann, Extracting object contours with the sweep of a robotic whisker using torque information. *Int. J. Robot. Res.* **29**, 1233–1245 (2010).

17. M. Kaneko, N. Kanayama, T. Tsuji, Active antenna for contact sensing. *IEEE Trans. Robot. Autom.* **14**, 278–291 (1998).

18. N. Ueno, M. M. Svinin, M. Kaneko, Dynamic contact sensing by flexible beam. *IEEE/ASME Trans. Mechatron.* **3**, 254–264 (1998).

19. F. A. Lucianna, A. L. Albarracín, S. M. Vrech, F. D. Farfán, C. J. Felice, The mathematical whisker: A review of numerical models of the rat◻s vibrissa biomechanics. *J. Biomech.* **49**, 2007–2014 (2016).

20. M. Seale, C. Cummins, I. M. Viola, E. Mastropaolo, N. Nakayama, Design principles of hair-like structures as biological machines. *J. R. Soc. Interface* **15**, 20180206 (2018).

21. H. M. Belli, A. E. T. Yang, C. S. Bresee, M. J. Z. Hartmann, Variations in vibrissal geometry across the rat mystacial pad: Base diameter, medulla, and taper. *J. Neurophysiol.* **117**, 1807–1820 (2017).

22. H. M. Belli, C. S. Bresee, M. M. Graff, M. J. Z. Hartmann, Quantifying the three-dimensional facial morphology of the laboratory rat with a focus on the vibrissae. *PLOS ONE* **13**, e0194981 (2018).

23. L. A. Huet, M. J. Z. Hartmann, The search space of the rat during whisking behavior. *J. Exp. Biol.* **217**, 3365–3376 (2014).

24. F. L. Rice, Structure, vascularization, and innervation of the mystacial pad of the rat as revealed by the lectin *Griffonia simplicifolia*. *J. Comp. Neurol.* **337**, 386–399 (1993).

25. L. Ibrahim, E. A. Wright, The growth of rats and mice vibrissae under normal and some abnormal conditions. *Development* **33**, 831–844 (1975).

26. D. P. Harland, J. A. Vernon, J. L. Woods, S. Nagase, T. Itou, K. Koike, D. A. Scobie, A. J. Grosvenor, J. M. Dyer, S. Clerens, Intrinsic curvature in wool fibres is determined by the relative length of orthocortical and paracortical cells. *J. Exp. Biol.* **221**, jeb172312 (2018).

27. E. Bertolazzi, M. Frego, G^1 fitting with clothoids. *Math. Methods Appl. Sci.* **38**, 881–897 (2015).

28. O. F. Chernova, V. F. Kulikov, Structural differences between the shafts of mammalian vibrissae and hairs and their causes. *Gen. Biol.* **438**, 182–185 (2011).

29. M. Abramowitz, I. A. Stegun, *Handbook of Mathematical Functions* (Dover, 1972).

30. S. A. Hires, A. Schuyler, J. Sy, V. Huang, I. Wyche, X. Wang, D. Golomb, Beyond cones: An improved model of whisker bending based on measured mechanics and tapering. *J. Neurophysiol.* **116**, 812–824 (2016).

Citation: E. L. Starostin, R. A. Grant, G. Dougill, G. H. M. van der Heijden, V. G. A. Goss, The Euler spiral of rat whiskers. *Sci. Adv.* **6**, eaax5145 (2020).

Science Advances

The Euler spiral of rat whiskers

Eugene L. Starostin, Robyn A. Grant, Gary Dougill, Gert H. M. van der Heijden and Victor G. A. Goss

ARTICLE TOOLS	http://advances.sciencemag.org/content/6/3/eaax5145
SUPPLEMENTARY MATERIALS	http://advances.sciencemag.org/content/suppl/2020/01/13/6.3.eaax5145.DC1
REFERENCES	This article cites 24 articles, 4 of which you can access for free http://advances.sciencemag.org/content/6/3/eaax5145#BIBL
PERMISSIONS	http://www.sciencemag.org/help/reprints-and-permissions

Use of this article is subject to the Terms of Service